Lawrence Berkeley National Laboratory

Title

Arrays of Fresnel Nanosystems for Enhanced Photovoltaic Performance.

Permalink

https://escholarship.org/uc/item/16b6f2jz

Journal

ACS Omega, 8(26)

Authors

Prajapati, Ashish
Shalev, Gil

Publication Date

2023-07-04

DOI

10.1021/acsomega.2c07863

Peer reviewed

Arrays of Fresnel Nanosystems for Enhanced Photovoltaic Performance

Ashish Prajapati and Gil Shalev*

ACCESS | Metrics & More | Article Recommendations

ABSTRACT: Omnidirectional broadband absorption of the solar radiation is pivotal to solar energy harvesting and particularly to low-cost non-tracking photovoltaic (PV) technologies. The current work numerically examines the utilization of surface arrays composed of Fresnel nanosystems (Fresnel arrays), which are reminiscent of the known Fresnel lenses, for the realization of ultra-thin silicon PV cells. Specifically, the optical and electrical performances of PV cells integrated with Fresnel arrays are compared with those of a PV cell incorporated with an optimized surface array of nanopillars (NP array). It is shown that the broadband absorption of specifically tailored Fresnel arrays can provide an enhancement of ∼20% over that of an optimized NP array. The performed analysis suggests that broadband absorption in ultra-thin films decorated with Fresnel arrays is driven by two light trapping mechanisms. The first is light trapping governed by light concentration, induced by the arrays, into the underlying substrates, which increases the optical coupling between the impinging illumination and the substrates. The second mechanism is light trapping motivated by refraction, as the Fresnel arrays induce lateral irradiance in the underlying substrates, which increases the optical interaction length and hence the overall probability for optical absorption. Finally, PV cells incorporated with surface Fresnel arrays are numerically calculated, with short-circuit current densities (J_{sc}) which are ∼50% higher than that of a PV cell incorporated with an optimized NP array. Also, the effect of increased surface area, due to the presence of Fresnel arrays, and its effect on surface recombination and open-circuit voltage (V_{oc}) are discussed.
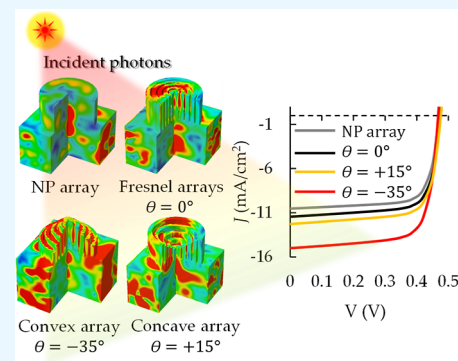
INTRODUCTION

Efficient light trapping and broadband absorption of the solar energy are important to various solar energy applications. Specifically, efficient broadband absorption of solar photons in an omnidirectional manner is important to low-cost non-tracking silicon photovoltaic (PV) technologies, which are required to competently harvest solar photons during the sun's diurnal path in the sky.[1−3] Also, efficient light trapping strategies to provide omnidirectional broadband solar absorption are required in order to realize silicon thin-film PV cells, which implies lower infrastructure and deployment costs, the potential to support flexible PV cells, and also the potential to support future realization of thin films based on expensive scarce materials, for example.

In his seminal work, Yablonovitch derived a geometrical optics description for efficient light trapping in thin films which is based on the decoration of both front and top surfaces. The outcome of his approach defines the known $4n^2$ limit, or the Yablonovitch limit, for light trapping in thin films (where n is the dielectric constant of the film).[4] More recently, it was suggested and demonstrated how the Yablonovitch limit can be exceeded with the employment of wave optics phenomena, and specifically the decoration of the thin film's surfaces with arrangements of subwavelength structures. The Fan group predicts that light trapping in thin films decorated with

photoinactive two-dimensional shallow grating can produce light trapping enhancement of $12n^2$.[5,6] Callahan et al. describe how to exceed the Yablonovitch $4n^2$ limit using an absorber of high optical density of states by the utilization of subwavelength structures.[7] Sturmberg et al. provide mode analysis for highly absorbing free-floating arrays of nanopillars (NP arrays), which is motivated by strong mode coupling with the incidence field, energy concentration by the individual NPs composing the arrays and excitations of Fabry−Perot modes.[8] Surface decoration with subwavelength structures in an ordered or disordered arrangements (metamaterials) of various geometries and materials have been demonstrated to provide excellent broadband and omnidirectional absorption of solar photons.[9−28] For example, surface arrays of subwavelength dimensions, such as NP arrays, nanocone arrays, light funnel arrays, etc., have been studied for their excellent light trapping mechanisms which provide enhanced solar absorption.[7,29−32]
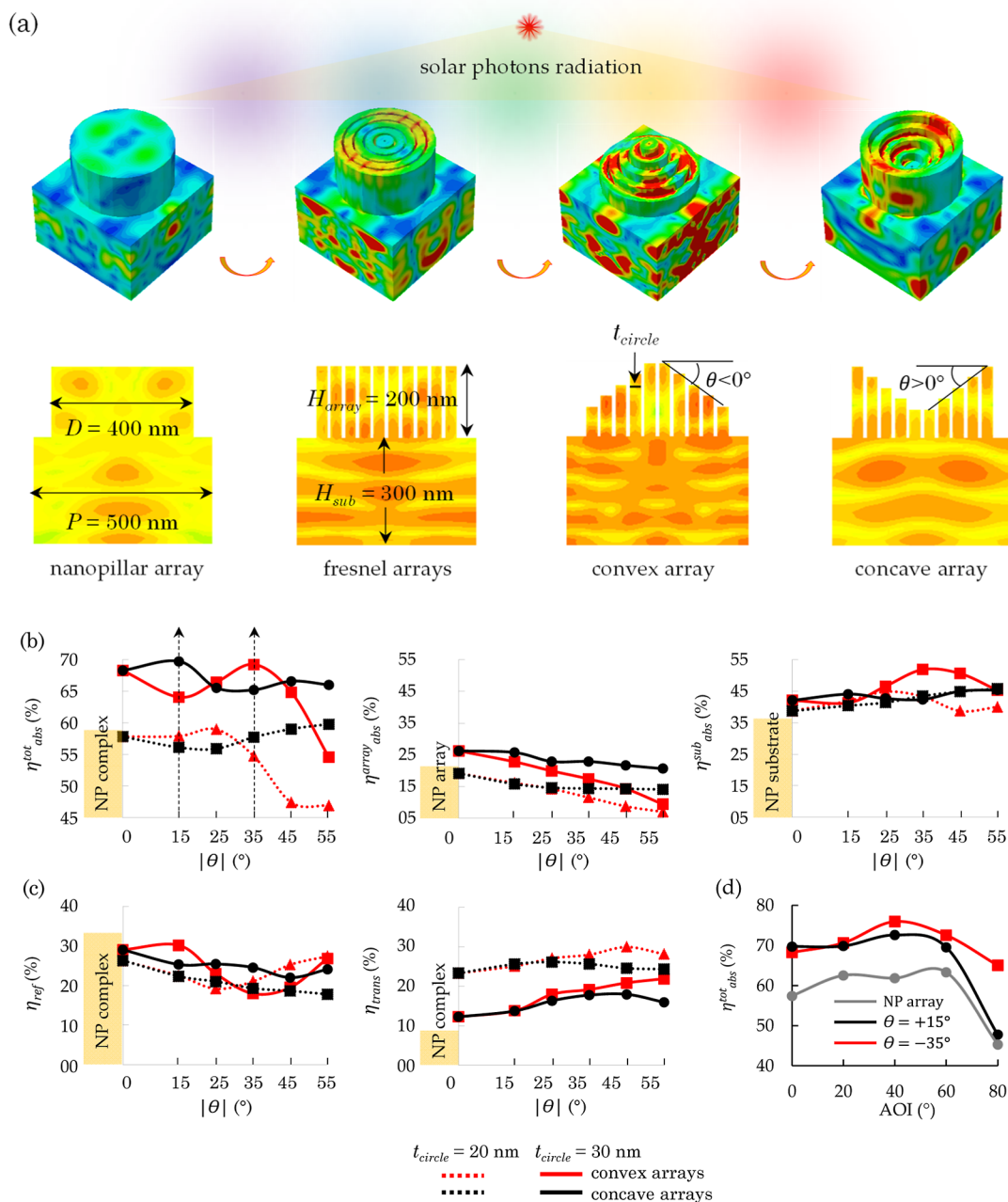
Figure 1. (a) Illustrations of the various considered Fresnel complexes with the relevant geometrical parameters. (b) θ-dependency of the broadband absorption of the full complexes, the arrays, and the substrates for the various considered geometries. (c) θ-dependency of the broadband reflection and the broadband transmission for the concave complex, the convex complex, NP complex, and $\theta = 0°$ complex. (d) AOI-dependency of the $\theta = -35°$ and the $\theta = 15°$ arrays (both with $t_{\text{circle}} = 30$ nm). Note: the NP complex is also shown for reference.

PV cells based on such approaches were realized with promising photocurrent performances.[19,20,33]

The current work examines the potential of surface decoration with arrays composed of silicon Fresnel nano-systems (Fresnel arrays) for omnidirectional broadband absorption of solar radiation. A single Fresnel nanosystem is inspired by the known, and much larger, Fresnel lens. The development of the known conventional Fresnel lens was spearheaded by the French scientist Augustin-Jean Fresnel for the purpose of serving in lighthouses.[34] Fresnel lenses are also discussed and utilized today for solar applications and specifically in the context of concentrated PVs.[35,36] The motivation for Fresnel lenses is twofold: (1) Fresnel lens allows

the realization of thin lenses with large apertures and short focal lengths of less material and volume to fit into lighthouses and (2) the need to efficiently collect light from the lighthouse source lamp, which propagates uniformly in all directions, and to redirect it toward the open seas such as to render it visible for ships over greater distances.[34] Compared with conventional lenses, the Fresnel lenses are less efficient in imaging but are particularly suited for non-imaging light concentration.[35,36] These properties of Fresnel lenses qualitatively motivate the current examination. Still, one has to keep in mind that the current work deals with arrays of Fresnel nanosystems rather than a single standalone Fresnel lens. This implies light trapping mechanisms associated with the optical interactions

between adjacent nanosystems, and mechanisms governed by wave optics phenomena such as diffraction and scattering from subwavelength particles.

METHODS

The three-dimensional electromagnetic calculations are performed with a finite-difference time-domain (FDTD) electromagnetic wave solver package by Synopsys Inc. The calculations are performed for infinite periodic arrays. A single unit cell is defined with periodic boundary conditions in the lateral directions and complementary matched layer boundary conditions in the vertical direction. Plane wave of a defined polarization is used for the optical excitation. The simulation space is divided into cells, each smaller than 10% of the exciting wavelength, in order to preserve accuracy. The magnetic and electric fields are calculated at the boundaries using the sine−cosine method with a phase shift which depends on the angle-of-incidence. The spatial distribution of the absorbed photon density and the optical generation are calculated for every wavelength at each cell. Sensors are located above and below the silicon complexes in order to count the reflected and transmitted photons. The broadband absorption is calculated by weighting the absorptivity with the AM1.5G solar spectrum standard. The broadband reflection and transmission are calculated similarly. The 400−900 nm spectra are calculated in 20 nm intervals. In order to ensure accuracy, the mesh size is set to values smaller than 1/10 of the wavelength in silicon.

The electrical performance is calculated with the Sentaurus Device package, also by Synopsys Inc. The Poisson and continuity equations are solved at each mesh point, accounting for the broadband optical generation profiles calculated using the FDTD method described above. Auger and Shockley−Read−Hall (SRH) recombination mechanisms are considered. The Auger recombination rate is calculated according to:[37] $R_{net}^{A} = (C_n n + C_p p)(np - n_{i,eff}^2)$, where the auger parameters C_n and C_p are fixed at 2.9×10^{-31} cm^6 s^{-1} and 1×10^{-31} cm^6 s^{-1}, respectively.[38] SRH recombination rate is calculated using:[37] $R_{net}^{SRH} = \frac{np - n_{i,eff}^2}{\tau_p(n + n_1) + \tau_n(p + p_1)}$, where n and p are the electron and hole charge carrier densities, $n_{i,eff}$ is the effective intrinsic density (considering bandgap narrowing), τ_n and τ_p are the electron and hole lifetimes, and n_1 and p_1 are calculated according to: $n_1 = n_{i,eff} \exp\left(\frac{E_{trap}}{kT}\right)$, $p_1 = n_{i,eff} \exp\left(\frac{-E_{trap}}{kT}\right)$, where E_{trap} is the energetic distance between the defect level and the intrinsic level and is fixed to zero. The optical constants of silicon are taken from ref 39.

RESULTS AND DISCUSSION

The considered silicon Fresnel arrays are composed of subwavelength Fresnel lenses in a square-tiled arrangement. The relevant geometrical parameters are presented in Figure 1a. In the following, we consider arrays on top of a 300 nm substrate (H_{sub}); the array's height (H_{array}) is set to 200 nm, and the period (P) is fixed at 500 nm. The starting geometry is the silicon NP array, which is optimized for the broadband absorption of the solar radiation with $P = 500$ nm and a NP diameter (D) of 400 nm.[17] The subwavelength Fresnel lenses are composed of concentric circles, which maintain the outer geometry and dimensions of the optimized NP, as shown in Figure 1a. The concavity and convexity of the Fresnel lens are

described by the angle θ (Figure 1a). $\theta > 0°$ reflects a concave array which is composed of subwavelength concave Fresnel lenses, and ($\theta < 0°$) reflects a convex array which is composed of subwavelength convex Fresnel lenses. In the following, we refer to a specific array by indicating its angle θ, and the substrate-array formations are referred to as complexes, followed by the θ value of the corresponding array. Similarly, the NP array and substrate formation are referred to as an NP complex. The height and diameter of the circles, composing the Fresnel lenses, are directly derived from the above geometrical parameters. The last geometrical parameter is the thickness of the circles (t_{circle}). In the following, we consider $t_{circle} = 20$ and 30 nm, such that for $t_{circle} = 20$, the gap between the circles is 20 nm, and for $t_{circle} = 30$ nm, the gap between the circles is 10 nm. Importantly, t_{circle} does not affect the height and diameter of the circles, and the transition from $t_{circle} = 20$ to 30 nm only implies that the distance between the concentric circles is smaller.

Figure 1b presents the θ-dependency of the broadband absorption under normal illumination for the Fresnel complexes, the arrays and the substrates. The broadband absorption of the NP complex, NP array, and NP substrate is also presented, correspondingly. Evidently, the mere transformation of the NP array into a Fresnel array can generate broadband absorption enhancement for the complexes which is higher than that of an optimized NP complex. In the present case, for the complexes under consideration, a maximum broadband absorption enhancement of ~20% is calculated for $\theta = 15°$ and $\theta = -35°$ complexes, both with $t_{circle} = 30$ nm.

The concave and convex complexes, and the $\theta = 0°$ complex, do not show any enhancement compared with the NP complex for $t_{circle} = 20$ nm, and broadband absorption even decreases for selected θ values. On the other hand, for $t_{circle} = 30$ nm, an absorption enhancement, compared with the NP complex, is demonstrated for almost all θ values, including for $\theta = 0°$, which generates broadband absorption not much different from the maximum absorption enhancements at $\theta = 15°$ and $\theta = -35°$ arrays. The importance of fill-factor (or volume material) is a well-recognized contributor to the broadband absorption in surface arrays of subwavelength structures,[17] and clearly the absorption of the $t_{circle} = 20$ nm arrays is always smaller than the corresponding absorption of the $t_{circle} = 30$ nm arrays. However, note that the substrate absorption of the $t_{circle} = 30$ nm complexes is always higher (or at least equal) than the absorption of the corresponding substrates of the $t_{circle} = 20$ nm complexes. This implies that the array fill-factor does not solely contribute to the array broadband absorption, but rather a higher array fill-factor also serves as a more efficient method to enhance substrate absorption. Also interesting, the concave complexes, for both $t_{circle} = 20$ nm and 30 nm, present a smaller θ-dependency compared with the convex complexes, which exhibit a significant decrease for $\theta > 35°$. This could be attributed to the intrinsic difference between the two complexes, which is associated with the nature of the two geometries: in a very broad manner, it is expected that the concave geometry induces more scattering inside the individual Fresnel nanolens, whereas the convex geometry is more susceptible to scattering between adjacent Fresnel nanolenses. In this manner, a higher θ value of a concave complex implies higher light trapping inside the individual Fresnel nanolens, whereas higher θ values of convex complexes suggest higher losses due to a higher sideway reflection by the Fresnel nanolenses.
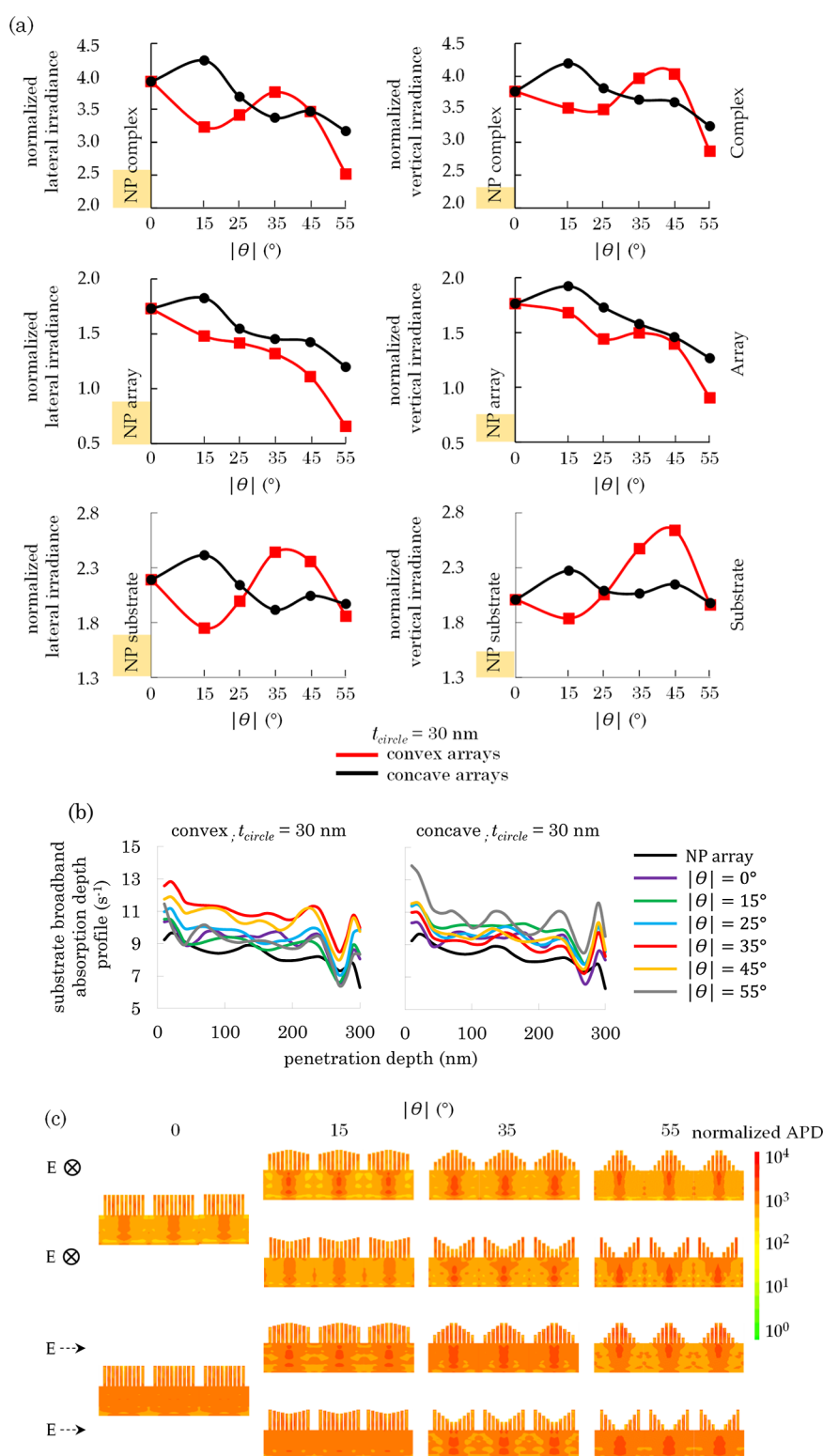
Figure 2. (a) θ-dependency of the lateral and vertical irradiance for the full complexes, for the arrays, and for the substrates. The NP array is also shown for reference. The arrow next to E reflects the direction of the impinging irradiance electric field. (b) θ-dependency of the broadband absorption depth profiles for convex and concave arrays, both with $t_{circle} = 30$ nm. The NP array is also shown for reference. The x-axis zero value marks the top of the substrate. (c) Cross-sections showing the normalized APD under broadband illumination for $\theta = 0$, 15, 35, and 55°.

Furthermore, also in Figure 1b, the broadband absorption enhancement is predominantly due to higher absorption in the substrates rather than the arrays, and a maximum broadband substrate absorption enhancement of 41%, for the $\theta = -35°$, $t_{circle} = 30$ nm array, is calculated with respect to the NP substrate. Evidently, the presence of Fresnel arrays induces a higher broadband absorption in the underlying substrates, which suggests that the Fresnel array functions as an enhanced optical mediator between the impinging illumination and the underlying substrates. Obviously, this agrees with the known
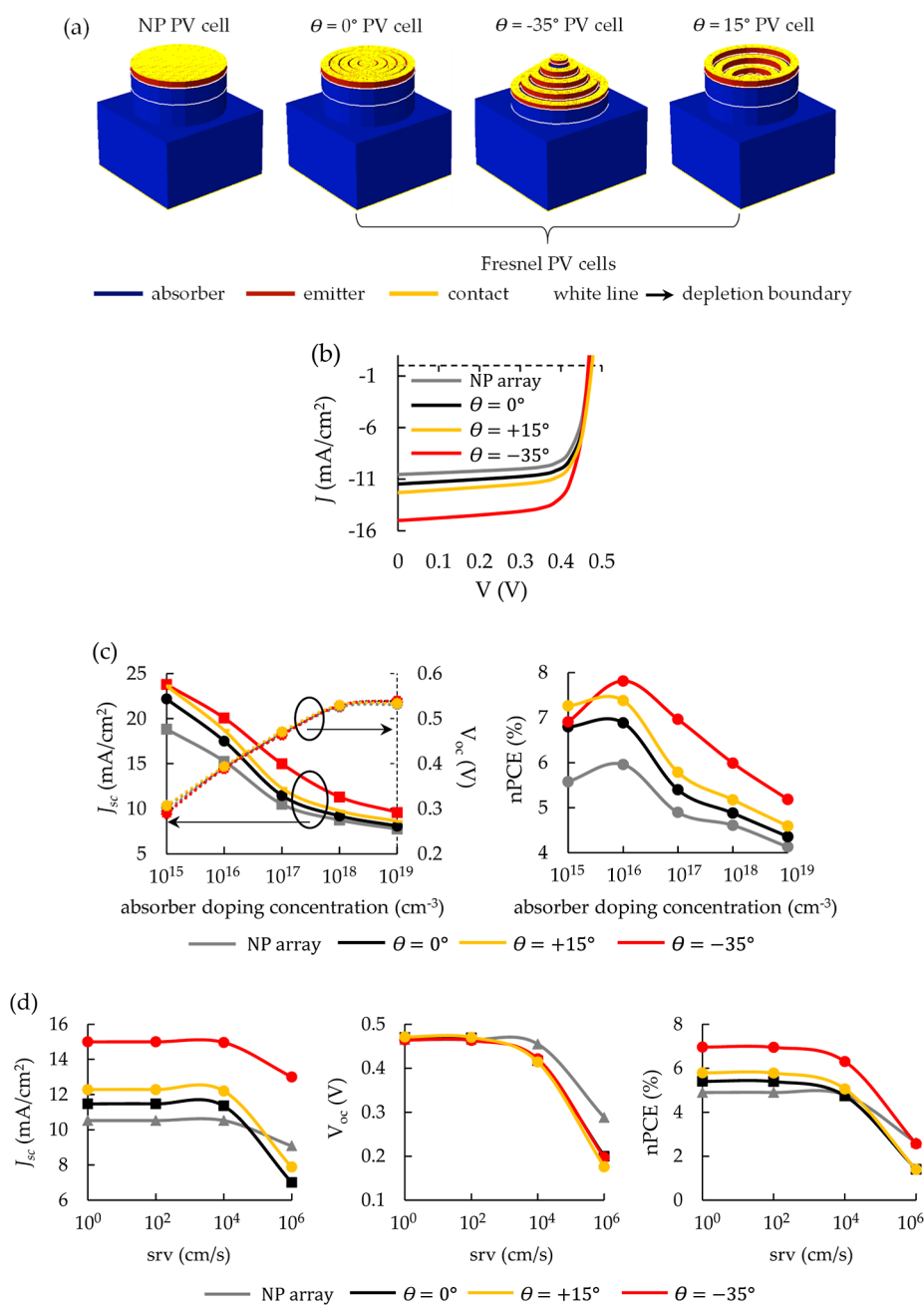
Figure 3. (a) Illustrations showing the considered PV cells. (b) I−V curves under broadband illumination for selected θ values and an absorber doping concentration of 10^{17} cm^{-3}. (c) Dependency of J_{sc}, V_{oc}, and nPCE on absorber doping level for the selected θ values. (d) SRV-dependency of J_{sc}, V_{oc}, and nPCE for the selected θ values.

non-imaging performance of conventional large-size Fresnel lenses.[35,36] The light trapping mechanisms triggered by the Fresnel arrays are discussed below in Figure 2.

Figure 1c presents the corresponding broadband reflection and transmission of the considered complexes. Clearly, all Fresnel arrays form efficient broadband anti-reflection coatings. The broadband reflection does not present any consistent behavior distinguishing between the various complexes. However, surprisingly, the complexes of t_{circle} = 20 nm present lower broadband reflection values for most θ values, which is inconsistent with the distinct higher broadband absorption for the t_{circle} = 30 nm complexes. This inconsistency is resolved by the examination of the broadband transmission. The distinct higher broadband absorption for the t_{circle} = 30 nm is

consistent with the broadband transmission values, as t_{circle} = 30 nm complexes exhibit consistent and distinct lower broadband transmission values. For example, the low broadband transmission of the θ = −35°, t_{circle} = 30 nm complex, coupled with a low broadband reflection, induces a high broadband absorption in the substrate (Figure 1b). The lower broadband transmission values of the t_{circle} = 30 nm complexes imply the enhanced light tapping in the substates, which is also implied in the broadband absorption of these (Figure 1b). Finally, Figure 1d presents the angle-of-incidence (AOI) dependency for the two complexes which perform best under normal illumination: the θ = −35° and the θ = 15° arrays, both with t_{circle} = 30 nm. The AOI-dependency of the NP complex is also presented. Note that overall, the AOI

dependency is enhanced for both the convex and concave complexes. Specifically, significant enhancement is presented for AOI = 80°, with almost 50% enhancement for the convex complex compared with the NP complex. The enhanced AOI dependency provided by the Fresnel arrays suggests a high density of asymmetric modes, which provide efficient coupling with the oblique irradiance.

Figure 2a shows the broadband directional distribution of the irradiance under normal illumination in the complexes, arrays, and substrates, all with t_{circle} = 30 nm. Evidently, the presence of Fresnel nanosystems induces a significant irradiance enhancement in both the lateral $(x−y)$ and vertical (z) directions for all θ values. The higher vertical and lateral irradiance for the $\theta = -35°$ and $\theta = 15°$ complexes is evident and consistent with the broadband absorption of these (Figure 1b). Also, consistent with Figure 1b, it is the high broadband irradiance enhancement in the substrates, both in the lateral directions and the vertical direction, which modulates the overall broadband absorption of the complexes. Noticeably, the total substrate irradiance stems from relatively equal contributions from the lateral and vertical irradiance. This suggests two interesting mechanisms of light trapping driven by the presence of surface arrays composed of Fresnel nanosystems: (1) light trapping governed by light concentration into the substrates, which is reflected in the high vertical irradiance; and (2) light trapping by refraction which explains the increased lateral irradiance.

In order to better understand the effect of surface Fresnel arrays on the substrate broadband absorption, Figure 2b presents the broadband absorption depth profiles in the substrates for t_{circle} = 30 nm under normal solar illumination. $\theta = -35°$ provides the highest substrate absorption for the convex substrate which is relatively uniform throughout the substrate. For the concave arrays, the highest substrate absorption depth profile is calculated for $\theta = 55°$, in agreement with Figure 1b, which shows that the corresponding substrate absorption is highest at $\theta = 55°$. Lastly, Figure 2c presents the spatial distributions of the absorbed photon density (APD) under broadband and normal solar illumination for selected values of θ. Note the enhanced substrate absorption for the $\theta = -35°$ convex complex and the $\theta = 55°$ concave complex which is consistent with the broadband absorption and the absorption depth profiles presented in Figures 1b and 2b, respectively. Also, these cross-sections clearly reflect the suggested light trapping mechanisms of light concentration and refraction.

Next, the PV performance of PV cells based on the suggested Fresnel arrays is numerically evaluated. Figure 3a presents the considered PV cells. The PV cell is composed of a single array unit cell, in which the optical generation is calculated for a unit cell nested in the array. In the current case, an axial junction configuration is considered with a 20 nm shallow degenerated n-type emitter (5×10^{19} cm^{-3}, phosphorus) and a p-type absorber (boron). In this way, the photoelectrons are collected at the top contact, and the photoholes are collected at the bottom contact. Figure 3b presents the calculated current−voltage $(I−V)$ curves under broadband solar illumination (AM1.5G). The absorber doping concentration is 10^{17} cm^{-3}. The considered geometries are: a NP array (NP PV cell), a Fresnel array of $\theta = 0°$ ($\theta = 0°$ PV cell), $\theta = -35°$ convex array ($\theta = -35°$ PV cell), and $\theta = 15°$ concave array ($\theta = 15°$ PV cell). The transition from NP and $\theta = 0°$ PV cells into the concave and convex PV cells clearly

shows the expected enhancement in short-circuit photocurrent (J_{sc}), with a maximum enhancement of ∼50% for the $\theta = -35°$ PV cell relative to the NP PV cell. Interestingly, the J_{sc} of the $\theta = -35°$ PV cell is significantly higher than that of the $\theta = 15°$ PV cell, although the broadband absorption of both complexes is very similar (Figure 1b). Therefore, the variation between the J_{sc} values must be related to the collection efficiency of the photo-carriers in each of the PV cells. This variation must be related to the contact configuration of the top emitter electrode, which differs between the two PV cells. Hence, the $\theta = -35°$ PV cell top emitter contact configuration provides an enhanced selectivity toward electrons as compared with the $\theta = 15°$ PV cell (meaning that photo-generated holes are less likely to reach the top emitter contact in the $\theta = -35°$ PV cell). Figure 3c presents the dependency of J_{sc} and open-circuit voltage (V_{oc}) on absorber doping concentration for the various considered PV cells. Note that, as expected, higher J_{sc} values are calculated for the lower absorber doping levels, and higher V_{oc} values are recorded for the higher doping levels. The J_{sc} enhancement, induced by the Fresnel arrays, is evident for all considered absorber doping levels, whereas, as expected, the transition from one surface array to the other does not affect V_{oc} values. Figure 3c also presents the nominal power conversion efficiency (nPCE), which is the conventional PV efficiency excluding the effect of serial and parallel resistances (fill-factor). It is shown that for the considered geometries, the optimal absorber doping is set at 10^{16} cm^{-3} which provides an enhancement of 33% for the $\theta = -35°$ PV cell in comparison with the NP cell. Finally, the main concern with surface decorations is the enhanced surface-volume-ratio which in thin-film PV cells translates directly to elevated surface recombination and consequential decrease in V_{oc}.[20,33] The dependency of J_{sc}, V_{oc}, and nPCE on surface recombination velocity (SRV) is presented in Figure 3d. The effect of SRV on J_{sc} is triggered for SRV values ∼10^4 cm/s, but the more important effect is with V_{oc} with a dramatic decrease for SRV > 10^4 cm/s. As expected, the NP PV cell is less affected by SRV as the NP surface is significantly smaller than the surface area of the Fresnel nanosystem. Note that recent publications demonstrated surface passivation, resulting in SRV values in the range of 1 cm/s.[40]

■ CONCLUSIONS

The notion of surface arrays composed of Fresnel nano-systems, for enhanced broadband and omnidirectional absorption of the solar radiation, is examined. Although the enhanced performance of PV cells incorporated with Fresnel arrays is numerically demonstrated, still, the realization of such PV cells remains challenging. Specifically, the fabrication of arrays composed of Fresnel nanosystems, considered in the current work, requires lithographic definition and etch processes of ultra-small features in the range of few dozen nanometers (i.e., t_{circle}), which obviously have cost implications (although current nanoimprint lithography technologies can address this challenge in a low-cost manner). In addition, any top conformal surface passivation/decoration is challenging as well. Overall, considering the fine details associated with the structure of the Fresnel nanosystems, the realization of any low-cost PV cell based on this approach is challenging. Still, the Fresnel arrays do offer interesting light trapping mechanisms employing light concentration and refraction. Hence, the presented work paves the way for future research to pursue

such light trapping mechanisms using geometries of a more relaxed design rules to support low-cost PV cells.

■ AUTHOR INFORMATION

Corresponding Author

Gil Shalev − School of Electrical and Computer Engineering, Ben-Gurion University of the Negev, Beer-Sheva 8410501, Israel; The Ilse-Katz Institute for Nanoscale Science and Technology, Ben-Gurion University of the Negev, Beer-Sheva 8410501, Israel; ● orcid.org/0000-0002-6893-1720; Email: glshalev@bgu.ac.il

Author

Ashish Prajapati − School of Electrical and Computer Engineering, Ben-Gurion University of the Negev, Beer-Sheva 8410501, Israel; Present Address: Electrical and Computer Engineering, University of California Davis, 95616, United States, and Berkeley Marvell NanoLab at CITRIS, University of California Berkeley, 94720, United States; ● orcid.org/0000-0001-7509-3801

Complete contact information is available at:
https://pubs.acs.org/10.1021/acsomega.2c07863

Notes

The authors declare no competing financial interest.

■ REFERENCES

(1) Fu, H.-C.; Ramalingam, V.; Kim, H.; Lin, C.-H.; Fang, X.; Alshareef, H. N.; He, J.-H. MXene-Contacted Silicon Solar Cells with 11.5% Efficiency. *Adv. Energy Mater.* **2019**, *9*, 1900180.

(2) Wang, H.-P.; Li, S.; Liu, X.; Shi, Z.; Fang, X.; He, J.-H. Low-Dimensional Metal Halide Perovskite Photodetectors. *Adv. Mater.* **2021**, *33*, 2003309.

(3) Yan, T.; Li, Z.; Cao, F.; Chen, J.; Wu, L.; Fang, X. An All-Organic Self-Powered Photodetector with Ultraflexible Dual-Polarity Output for Biosignal Detection. *Adv. Mater.* **2022**, *34*, 2201303.

(4) Yablonovitch, E. Statistical Ray Optics. *J. Opt. Soc. Am.* **1982**, *72*, 899.

(5) Yu, Z.; Raman, A.; Fan, S. Fundamental Limit of Light Trapping in Grating Structures. *Opt. Express* **2010**, *18*, A366−A380.

(6) Yu, Z.; Raman, A.; Fan, S. Fundamental Limit of Nanophotonic Light Trapping in Solar Cells. *Proc. Natl. Acad. Sci. U.S.A.* **2010**, *107*, 17491−17496.

(7) Callahan, D. M.; Munday, J. N.; Atwater, H. a. Solar Cell Light Trapping beyond the Ray Optic Limit. *Nano Lett.* **2012**, *12*, 214−218.

(8) Sturmberg, B. C. P.; Dossou, K. B.; Botten, L. C.; Asatryan, A. A.; Poulton, C. G.; McPhedran, R. C.; de Sterke, C. M. Absorption Enhancing Proximity Effects in Aperiodic Nanowire Arrays. *Opt. Express* **2013**, *21*, A964−A969.

(9) Hu, L.; Chen, G. Analysis of Optical Absorption in Silicon Nanowire Arrays for Photovoltaic Applications. *Nano Lett.* **2007**, *7*, 3249−3252.

(10) Spinelli, P.; Verschuuren, M. A.; Polman, A. Broadband Omnidirectional Antireflection Coating Based on Subwavelength Surface Mie Resonators. *Nat. Commun.* **2012**, *3*, 692.

(11) Kim, S. K.; Zhang, X.; Hill, D. J.; Song, K. D.; Park, J. S.; Park, H. G.; Cahoon, J. F. Doubling Absorption in Nanowire Solar Cells with Dielectric Shell Optical Antennas. *Nano Lett.* **2015**, *15*, 753−758.

(12) Li, Y.; Li, M.; Fu, P.; Li, R.; Song, D.; Shen, C.; Zhao, Y. A Comparison of Light-Harvesting Performance of Silicon Nanocones and Nanowires for Radial-Junction Solar Cells. *Sci. Rep.* **2015**, *5*, 11532.

(13) Wong, A. B.; Brittman, S.; Yu, Y.; Dasgupta, N. P.; Yang, P. Core-Shell CdS-Cu2S Nanorod Array Solar Cells. *Nano Lett.* **2015**, *15*, 4096−4101.

(14) Nowzari, A.; Heurlin, M.; Jain, V.; Storm, K.; Hosseinnia, A.; Anttu, N.; Borgström, M. T.; Pettersson, H.; Samuelson, L. A Comparative Study of Absorption in Vertically and Laterally Oriented InP Core-Shell Nanowire Photovoltaic Devices. *Nano Lett.* **2015**, *15*, 1809−1814.

(15) Wallentin, J.; Anttu, N.; Asoli, D.; Huffman, M.; Aberg, I.; Magnusson, M. H.; Siefer, G.; Fuss-Kailuweit, P.; Dimroth, F.; Witzigmann, B.; Xu, H. Q.; Samuelson, L.; Deppert, K.; Borgström, M. T. InP Nanowire Array Solar Cells Achieving 13.8% Efficiency by Exceeding the Ray Optics Limit. *Science* **2013**, *339*, 1057−1060.

(16) Aberg, I.; Vescovi, G.; Asoli, D.; Naseem, U.; Gilboy, J. P.; Sundvall, C.; Dahlgren, A.; Svensson, K. E.; Anttu, N.; Bjork, M. T.; et al. A GaAs Nanowire Array Solar Cell with 15.3 % Efficiency at 1 Sun. *IEEE J. Photovoltaics* **2016**, *6*, 185−190.

(17) Shalev, G.; Schmitt, S.; Brönstrup, G.; Christiansen, S. Maximizing the Ultimate Absorption Efficiency of Vertically-Aligned Semiconductor Nanowire Arrays with Wires of a Low Absorption Cross-Section. *Nano Energy* **2015**, *12*, 801−809.

(18) Huang, Y.-F.; Chattopadhyay, S.; Jen, Y.-J.; Peng, C.-Y.; Liu, T.-A.; Hsu, Y.-K.; Pan, C.-L.; Lo, H.-C.; Hsu, C.-H.; Chang, Y.-H.; Lee, C.-S.; Chen, K.-H.; Chen, L.-C. Improved Broadband and Quasi-Omnidirectional Anti-Reflection Properties with Biomimetic Silicon Nanostructures. *Nat. Nanotechnol.* **2007**, *2*, 770−774.

(19) Jeong, S.; McGehee, M. D.; Cui, Y. All-Back-Contact Ultra-Thin Silicon Nanocone Solar Cells with 13.7% Power Conversion Efficiency. *Nat. Commun.* **2013**, *4*, 2950.

(20) Savin, H.; Repo, P.; von Gastrow, G.; Ortega, P.; Calle, E.; Garín, M.; Alcubilla, R. Black Silicon Solar Cells with Interdigitated Back-Contacts Achieve 22.1% Efficiency. *Nat. Nanotechnol.* **2015**, *10*, 624−628.

(21) Brongersma, M. L.; Cui, Y.; Fan, S. Light Management for Photovoltaics Using High-Index Nanostructures. *Nat. Mater.* **2014**, *13*, 451−460.

(22) Garnett, E.; Yang, P. Light Trapping in Silicon Nanowire Solar Cells. *Nano Lett.* **2010**, *10*, 1082−1087.

(23) Martins, E. R.; Li, J.; Liu, Y.; Depauw, V.; Chen, Z.; Zhou, J.; Krauss, T. F. Deterministic Quasi-Random Nanostructures for Photon Control. *Nat. Commun.* **2013**, *4*, 2665.

(24) van Lare, M.-C.; Polman, A. Optimized Scattering Power Spectral Density of Photovoltaic Light-Trapping Patterns. *ACS Photonics* **2015**, *2*, 822−831.

(25) Gaucher, A.; Cattoni, A.; Dupuis, C.; Chen, W.; Cariou, R.; Foldyna, M.; Lalouat, L.; Drouard, E.; Seassal, C.; Roca I Cabarrocas, P.; Collin, S. Ultrathin Epitaxial Silicon Solar Cells with Inverted Nanopyramid Arrays for Efficient Light Trapping. *Nano Lett.* **2016**, *16*, 5358−5364.

(26) Fountaine, K. T.; Cheng, W.-H.; Bukowsky, C. R.; Atwater, H. A. Near-Unity Unselective Absorption in Sparse InP Nanowire Arrays. *ACS Photonics* **2016**, *3*, 1826−1832.

(27) Marko, G.; Prajapati, A.; Shalev, G. Subwavelength Nonimaging Light Concentrators for the Harvesting of the Solar Radiation. *Nano Energy* **2019**, *61*, 275−283.

(28) Prajapati, A.; Llobet, J.; Antunes, M.; Martins, S.; Fonseca, H.; Calaza, C.; Gaspar, J.; Shalev, G. An Efficient and Deterministic Photon Management Using Deep Subwavelength Features. *Nano Energy* **2020**, *70*, 104521.

(29) Yu, Z.; Raman, A.; Fan, S. Fundamental Limit of Light Trapping in Grating Structures. *Opt. Express* **2010**, *18*, A366−A380.

(30) Sturmberg, B. C. P.; Dossou, K. B.; Botten, L. C.; Asatryan, A. A.; Poulton, C. G.; de Sterke, C. M.; McPhedran, R. C. Modal Analysis of Enhanced Absorption in Silicon Nanowire Arrays. *Opt. Express* **2011**, *19*, A1067.

(31) Chauhan, A.; Prajapati, A.; Calaza, C.; Fonseca, H.; Sousa, P. C.; Llobet, J.; Shalev, G. Near-Field Optical Excitations in Silicon Subwavelength Light Funnel Arrays for Broadband Absorption of the Solar Radiation. *Sol. RRL* **2021**, *5*, 2100721.

(32) Chauhan, A.; Prajapati, A.; Llobet, J.; Fonseca, H.; Sousa, P. C.; Calaza, C.; Shalev, G. Incorporation of Nano-Features into Surface

Photoactive Arrays for Broadband Absorption of the Solar Radiation. *Sol. Energy Mater. Sol. Cells* **2022**, *245*, 111864.

(33) Oh, J.; Yuan, H.-C.; Branz, H. M. An 18.2%-Efficient Black-Silicon Solar Cell Achieved through Control of Carrier Recombination in Nanostructures. *Nat. Nanotechnol.* **2012**, *7*, 743−748.

(34) Leutz, R.; Suzuki, A. *Nonimaging Fresnel Lenses*; Springer Berlin, Heidelberg: Berlin Heidelberg, 2001.

(35) Miller, D. C.; Kurtz, S. R. Durability of Fresnel lenses: A review specific to the concentrating photovoltaic application. *Sol. Energy Mater. Sol. Cells* **2011**, *95*, 2037−2068.

(36) Xie, W. T.; Dai, Y.; Wang, R. Z.; Sumathy, K. Concentrated Solar Energy Applications Using Fresnel Lenses : A Review. *Renewable Sustainable Energy Rev.* **2011**, *15*, 2588−2606.

(37) Sze, S. M. *Physics of Semiconductor Devices*, 2nd ed.; Wiley: New York, 1981.

(38) Lochmann, W.; Haug, A. Phonon-assisted Auger recombination in Si with direct calculation of the overlap integrals. *Solid State Commun.* **1980**, *35*, 553−556.

(39) Green, M. A.; Keevers, M. J. Optical Properties of Intrinsic Silicon at 300 K. *Prog. Photovoltaics Res. Appl.* **1995**, *3*, 189−192.

(40) Hoex, B.; Heil, S. B. S.; Langereis, E.; van de Sanden, M. C. M.; Kessels, W. M. M. Ultralow Surface Recombination of C-Si Substrates Passivated by Plasma-Assisted Atomic Layer Deposited Al2O3. *Appl. Phys. Lett.* **2006**, *89*, 042112.